Journal of Mechanical Engineering Research and Developments
ISSN: 1024-1752
CODEN: JERDFO
Vol. 44, No. 7, pp. 269-288
Published Year 2021

A Study of The Kinetics of Phase Precipitation When Aging Al-Mg-Si Alloy

Tan Sang Le[†], Nguyen Duong Nam[‡*], Vu Anh Tuan[‡], Thi Minh Hao Dong[‡†], Dinh Tuyen Nguyen[‡†*]

[†] Institute of Engineering, Ho Chi Minh city University of Technology (HUTECH), Ho Chi Minh city, Vietnam
[‡] Schoolo of Mechanical Engineering, Vietnam Maritime University, Haiphong, Vietnam
[‡†] Institute of Maritime, Ho Chi minh city University of Transport, Ho Chi Minh city, Vietnam

*Corresponding author email: namnguyenduong1985@gmail.com; nguyendinhtuyen8899@gmail.com

ABSTRACT

In this research, the results of kinetic study of phase precipitation on aging Al-Mg-Si alloy are presented. The results of the kinetic analysis of the process show that the formation of phases in the alloy is explained by the phase transformation kinetics. By the calculation results based on the hardness value, the coefficients K, n, Q were determined at different temperatures and aging times. The determination of these coefficients helps to determine the formation of phases in aging conditions. Also by the method of hardness measurement, the functions of phase transformation kinetics have been determined as well as the formation of different phases at each aging temperature of the studied alloy. Determining the kinetics of the phase formation when aging plays an important role in determining the formation as well as controlling the phase formation under different conditions.

KEYWORDS

solid solution, hardening, kinetics, thermodynamic, phase transformation, coeffcients

INTRODUCTION

The Al - Mg - Si heat-treated deformed aluminum alloy is strengthened on the basis of creating a oversaturated solid solution and the dispersed phase decomposition immediately afterwards has a hardening effect. Types of heat treatment are annealing, quenching and aging [1]–[4]. The first heat treatment operation is uniform annealing to increase the uniformity of the components which increase ductility for the subsequent plastic deformation process. The uniform annealing temperature is lower than the eutectic temperature and higher than the solubility limit of the alloying element in the α solid solution, usually an annealing temperature in the range 450 - 540^0C. The soaking time depends on the sample size, the size of the second element, normally lasts from 4 to 10 hours [5]–[9][10][11]. Quenching is the process of making a oversaturated solid solution for subsequent strengthening by precipitation aging of the dispersed phase. The alloy is heated to the quenching temperature (point A, figure 1), keeping the heat to dissolve the second phase molecules and homogenize the solid solution composition α. After cooling in water, the microstructure of alloy is a oversaturated solid solution (point B, figure 1). This is essential for the subsequent aging process [12]–[16]. After quenching, the alloy has structure as a oversaturated solid solution with a insignificant strengthening effect. To increase strengthening, it need to aging at a certain temperature and time, then the solid solution decomposition occurs, the microstructure of the alloy becomes two phases.

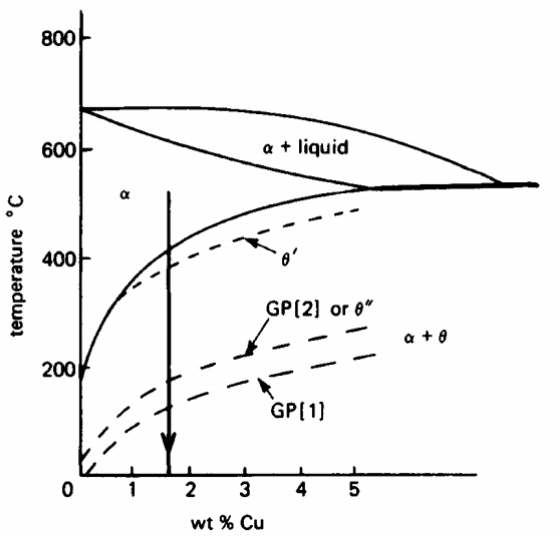

Figure 1. Diagram illustrating the phase transformation when quenching [17]

With increasing temperature (or lasting the soaking time at constant temperature), the microstructure transformation of the oversaturated solid solution begins with the formation of Guinier - Preston (GPZ) regions, next is the formation of β" phase (GPZ 2), β' phase và β phase (Mg_2Si) [18]–[25].

$\alpha_{qbh} \rightarrow$ GPZ $\rightarrow$ β' $\rightarrow$ β [4]

Guinier-Preston Zone (GPZ).

The microstructure of the alloy after quenching is a saturated solution of the alloying elements and the vacancy. The vacancies bind to surrounding alloying elements and form vacancy-alloy-element conjugates, which easily translocate, diffusing to the site of VGP formation. The GPZ is a region of oversaturated solid solution enriched with an alloying element, which of course has the same crystal structure as the solid solution. There is no clear boundary between VGP and the phase matrix. The shape of the GPZ region is different in different alloy systems, depending on many factors, the most important being the atomic size deviation, table 1. Due to the difference in atomic diameter Δd between Al and the element alloys, the formation of GP zone causes a rather large elastic stress field.

Table 1. Shape of GPZ at other alloys [26]

Shape of GPZ	Alloys	Differents of diameter atoms %
Spherical	Al – Ag	+ 0,7
	Al – Zn	- 1,9
	Al – Zn – Mg	+ 2,6
	Cu – Co	- 2,8
Disc	Al – Cu	- 11,8
	Cu – Be	- 8,8
Needle	Al – Mg – Si	+ 2,5
	Al – Cu – Mg	- 6,5

The size of GP zone is about 10÷100 A^0 depending on alloy composition, temperature and aging time.

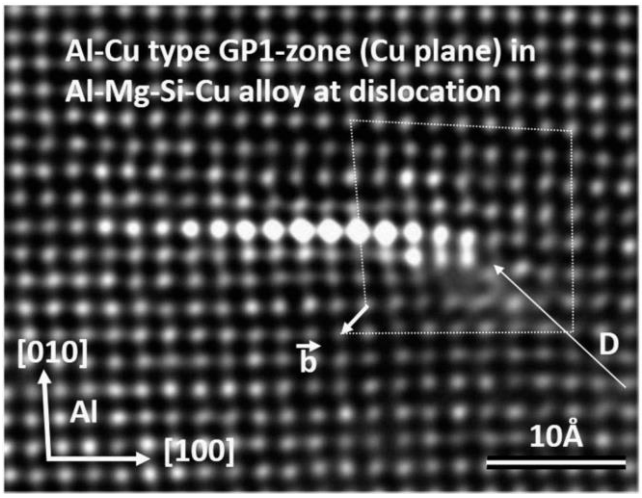

Figure 2. Guinier - Preston Zone [27]

In terms of thermodynamics, GPZ is similar to the pseudo-stable phase state and completely different from the region produced by component fluctuations. While the component fluctuations are unstable, the GPZ is stable over time. Similar to the thermodynamically stable phase, on the phase diagram, there is a dissolution curve of GPZ. GPZ can grow by annexing small neighboring regions by diffusion mechanism. The composition of GPZ at a given temperature is independent of the alloy composition. Comparing the dislocation density and the GPZ density when aging, it is found that the GPZ density is larger than the dislocation density [28]–[31]. On that basis, it is assumed that GPZ is generated by the co-phase nucleation mechanism on the concentration undulary regions. Thus, the GPZs are fairly evenly distributed over the entire sample volume.

β’ phase

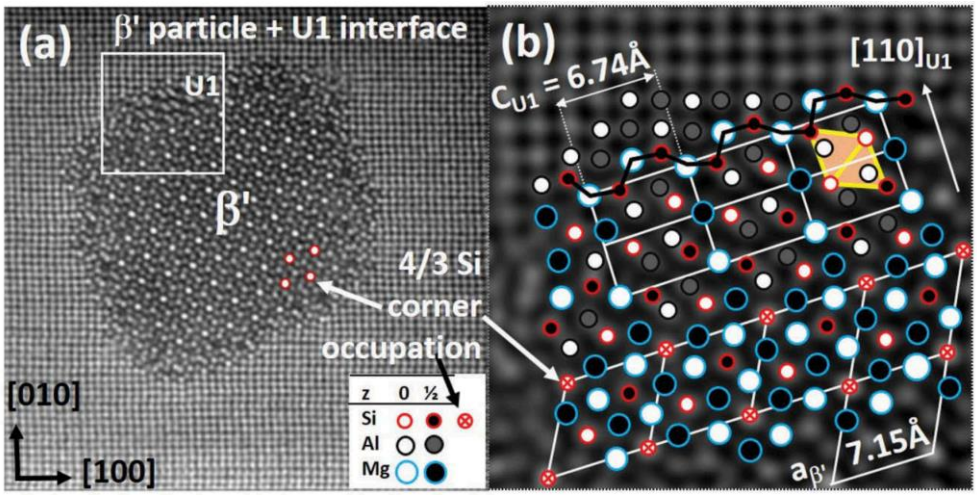

Figure 3. The pseudo-stable phase *β'*[27]

The β' phase has the corresponding composition Mg_2Si, the tetragonal type (Figure 3) with the crystal structure parameters a = 0.705 nm; c= 0.405 nm [4]. Between β' and α is only partially connected (Figure 4). The β' phase is rod-shaped. The elastic stress field generated by the generation of GPZ and the β" phase is larger than that of the β' phase [29], [32], [33].

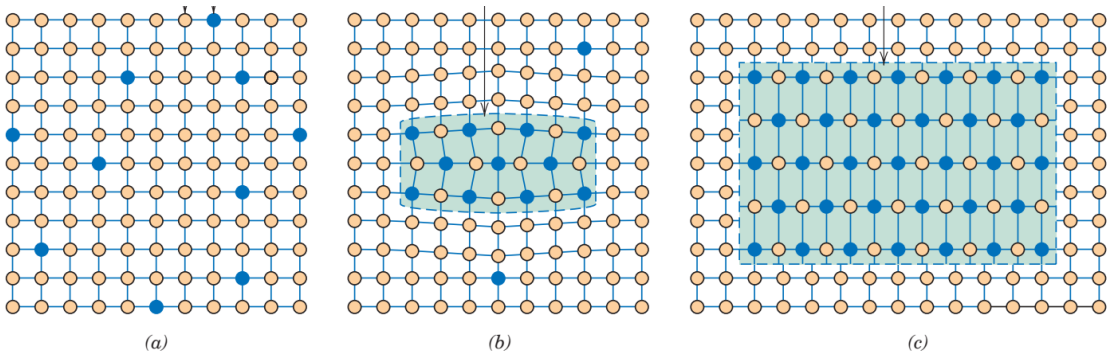

Figure 4. Crystall structure diagram:a- solid solution α; b- phase β'' is connected to α; c- phase β is stable independent of α. [34]

β (Mg_2Si) phase

The final period of the aging phase precipitation process of the 6xxx-system aluminum alloy is the formation of β (Mg_2Si) equilibrium phase structures and the grain coarsening of the β phase. The β phase (Mg_2Si) is a completely independent phase of the matrix (matrix), the square lattice type with lattice parameters a = 28.13 Ao (Figure 4c). About the nucleation mechanism of the β'' and β' phases, it is assumed that they are produced above dislocations, small grain boundaries, defects, and in the vacancies regions, at the same time they are also generated from the initial phase (morphomorphic transformation) for example GPZ → β'' or β''→ β' etc. So about the order of phases pha β'', β' can be generated by continuing to develop VGPs or can be generated completely independently of those regions. The β phase (Mg_2Si) too, can inherit the intermediate phases β'', β or can also be generated independently of those phases.

Studying the phase precipitation process when aging aluminum alloys by transmission electron microscope is one of the most effective methods [18][35]–[38]. However, direct study of phase secretion by transmission electron microscopy is not always easy to perform and with equipment conditions. On the other hand, by this method it is difficult to determine the kinetic parameters. There have been many studies on the decomposition of oversaturated solid solutions in aluminum. The authors all believe that the stable phase in the Al - Mg - Si alloy is Mg2Si with a face center cubic lattice, with lattice parameter a = 28.13 A0 . This compound in the Al - Mg - Si system is denoted by the β phase. In addition to the β phase, in technical alloys there may also be Al_6Mn phases; Mg_2Al_3…Most authors [28], [30], [39]–[45]believe that the decomposition of supersaturated solid solution occurs as follows:

Supersaturated solid solution Al_α → GP region → β' phase →β phase.

However, depending on the degree of oversaturation, the aging temperature and the number of stable phases may vary. In this study, the hardness measurement method was used to determine the aging kinetic characteristics: phase fraction (X), kinetic coefficients (K), and phase transformation activity (Q) from which to deduce the characteristics of nucleation and nucleation development in the aging process of Al - Mg - Si alloys.

FACTORS AFFECTING THE PHASE PRECIPITATION PROCESS

The phase precipitaion process is influenced by many factors. The factors that directly affect the phase precipitation kinetics are temperature, time, chemical composition and microstructure of the alloy before aging.

* Effects of temperature and aging time:

The strength and hardness of the alloy increase with increasing aging time, reaching a maximum and then decreasing [5-9][28][30][39]–[46]. The curve of change in strength (hardness) with aging time can be divided into two parts. The maximum left is the strengthening the right maximum corresponds to the over aging. With the 6xxx-system deformed aluminum alloy, with the maximum strength corresponding to the microstructure including GPZ, the intermediate phase is pseudo-stable β'with a certain ratio. Corresponding to the strength

removal state, the microstructure is the stable phase β is accumulating. The higher the aging temperature, the shorter the time to reach the maximum strength and of course the earlier the aging period occurs.

* Influence of alloy microstructure before aging:

- The effect of the vacancy: At the quenching temperature, the number of vacancies is quite large, when cooled rapidly they are retained in the solid solution α_{qbh} . The vacancies bind to the alloying element to form the conjugates that form the GPZ. The vacancy concentration in the vicinity of the grain boundary is strongly reduced by the diffusion process and self-destruction of the vacancy on the grain boundary. Because the vacancy concentration falls below the critical value, phase precipitation does not occur, resulting in a white region around grain boundary. Thus, the empty vacancies the role of promoting diffusion, enhancing phase precipitation, and is a necessary factor for phase precipitation to occur.

-Effect of dislocation: Dislocation affects the dynamics of the phase precipitation process, around which there is a stress field. To reduce the energy of the system due to the existence of these stress fields, the atoms of the alloying element tend to be distributed in the regions around the dislocation. Thus dislocation is one of the important factors causing the heterogeneity of the oversaturated solid solution after quenching. The Cottrell zones are the nucleation centers for the formation of GPZ and the intermediate phase. Plastic deformation increases the dislocation density thus promoting phase precipitation.

- Effects of defects: The generation of defects is associated with the change in the order of the tightly packed surface distribution, the crystal structure in the defects region is also different, the solubility of the alloying element between the solid solution and this lattice bias region is different. Therefore, in the misalignment region, the differentiation process will take place. These defects not only promotes phase precipitation, it also changes the crystal lattice of the precipitated phase.

- Effect of grain boundary and block grain boundary: The nucleation activity at the grain boundary is generally small because then the elastic and surface energies are small. Due to this feature, the differentiation process will not be the same at the grain boundary and inside the grain. The block grain boundary also has the effect of promoting phase precipitation.

Thus, by considering the influence of alloy microstructure before aging, we can see that plastic deformation increases the concentration of empty atoms, increases the increasing dislocation density, and increases thegrain boundary length and increase the density of defects, so it strongly affects the kinetics of the phase precipitation.

* Influence of alloy composition: The content of alloying elements is directly related to the solid solution oversaturation after quenching, the greater the overrsaturation, the greater the solid solution mechanical properties after quenching. On the other hand, when aging, the strengthened phase density precipitated in the alloy is higher when the oversaturation is greater. Combining the above two effects to explain the increase in hardness and strength of the alloy when increasing the content of alloying elements.

PHASE TRANSFORMATION DYNAMIC

The phase transformation kinetics is a matter of the relationship between the transformation phase mass and the transformation time. We set the phase transformation ratio to be (X), the phase transformation time is (t), then:

$$X = f(t) \quad (1)$$

Mean:

Volume of product phase/Total volume that can be phased

= Number of atoms in the product phase/Total number of atoms that can change phase

The volume of phase that can be transformed can be equal to the initial phase volume of the crystallization process (or eutectoid process), recrystallization or it can be just is a part (volume of oversaturated phase in phase precipitation).

Expression of experience

$X = 1 – \exp (- K . t^n)$ (2)

$K = k^n$

Equation (2) describes the dependence of the phase precipitation fraction X on time (t) and the phase transformation rate constant k , [1/sec].

K depends on the nucleation rate ($n_{nucleation}$) and the develop nucleation rate ($v_{develop}$),, the larger the k, the faster the phase transformation time, ie, t_{start} (small phase transformation time).

n - dimensionless coefficient, depends on the nucleation geometry, nucleation conditions.

We can determine the coefficients K and n based on experiment. X at different times can be determined by thermal analysis, optical microscopic_, hardness method and other physical methods such as resistance, stretching bloom, magnetic, or Xray.

From the X values found with the help of a computer, it is easy to determine the coefficients K and n.

Kinetics of phase transition in balanced phaseprecipitation

The following is derived by theoretical expression kinetics of phase precipitation, considering phase secretion β from a oversaturated solid solution α at temperature T.

X = Number of atoms in phase / Number of atoms that can form phase (3)

Consider the precipitated phase to be a sphere of radius r and all nuclears are generated from the initial time with an amount of N; volume of a nucleus $4\pi r^3/3$; The additional concentration in the precipitated phase volume region is (C_β - $C_{\alpha\beta}$) and the concentration that can participate in phase precipitation is (C_0 - $C_{\alpha\beta}$) then:

$$X_0 = \frac{4/3\pi r^3 N(C_\beta - C_{\alpha\beta})}{(C_0 - C_{\alpha\beta})} \quad (4)$$

Here X0 is X when X<<1, expression (3.4) can be written as:

$$r = \left[\frac{3X_0(C_0 - C_{\alpha\beta})}{4\pi N(C_\beta - C_{\alpha\beta}} \right]^{1/3} \quad (5)$$

From (4) and (5) we have:

$$\frac{dX_0}{dt} = 4\pi r^2 \frac{dr}{dt} N \frac{(C_\beta - C_{\alpha\beta})}{(C_0 - C_{\alpha\beta})} \quad (6)$$

On the other hand:

$$\frac{dr}{dt} = v_{phattrien} = \frac{D}{r} \cdot \frac{(C_0 - C_{\alpha\beta})}{(C_\beta - C_{\alpha\beta})} \quad (7)$$

Substituting (7) into (6) get:

$$\frac{dX_0}{dt} = 4\pi r^2 \frac{D}{r}.\frac{(C_0 - C_{\alpha\beta})}{(C_\beta - C_{\alpha\beta})} N \frac{(C_\beta - C_{\alpha\beta})}{(C_0 - C_{\alpha\beta})} = 4\pi r DN$$

$$= 4\pi \left[\frac{3X_0 (C_0 - C_{\alpha\beta})}{4\pi N (C_\beta - C_{\alpha\beta}} \right]^{1/3} DN \quad (8)$$

Set $K^{2/3} = \left[\frac{48.\pi^2 (C_0 - C_{\alpha\beta})}{(C_0 - C_{\alpha\beta}} \right]^{1/3} DN^{2/3}$

We have: $\frac{dX_0}{dt} = K^{2/3} X_o^{1/3}$ (9)

$$X_0^{-1/3} dX_0 = K^{2/3} dt$$
$$\Rightarrow X_0^{2/3} = K^{2/3} t \Rightarrow X_0 = Kt^{3/2}$$

Table 2. Coefficient n in phase precipitation

STT	Phase precipitation conditions	n
1	Nuclears develop in three directions:	
	With $n_{nucleation}$= 0	3/2
	With $n_{nucleation}$ = const	5/2
	With $n_{nucleation}$ ascending	>5/2
	With $n_{nucleation}$ descending	3/2÷5/2
2	Cylindrical nuclears, growing in 2 directions	
	With $n_{nucleation}$ = 0	2
	With $n_{nucleation}$ = const	3
	With $n_{nucleation}$ ascending	>3
	With $n_{nucleation}$ descending	2÷3
3	Disc-shaped nuclears	
	With $n_{nucleation}$ = 0	1
	With $n_{nucleation}$ = const	2
	With $n_{nucleation}$ ascending	>2
	With $n_{nucleation}$ descending	1÷2

Expression (10) is only true when the influence of matrix concentration on the growth of the grain is not taken into account, because then the concentration in the matrix for diffusion to the grain under consideration decreases, then X_0 is replaced by X. with the following characteristics:

thus: $\ln (1-X) = -X_0 = -K.t^{3/2}$ (12a)

or: $X = 1 - \exp (- K. t^n)$ (12b)

With time factor n = 3/2

K - rate coefficient, depending on nucleation and nucleation development conditions, n can have different values. From Table 2 it is shown that if n and K are determined experimentally, the characteristics of phase precipitation can be predicted and from K determine the Q phase precipitation activity.

Determination of phase precipitation activity

Method to determine the phase precipitation activity (Q).

The speed factor K is expressed by the formula:

$$K = const.exp(\frac{Q_{create\ phase}}{RT}) \quad (13)$$

The graph of the lnK function from (3.13) has the form as shown in Figure 8

From expressions (12b) and (13) we see:

The phase precipitation activity (Q) can be determined in terms of the phase transformation kinetic coefficient (K), or the phase transformation fraction (x).

Determination of phase precipitation activity from phase transformation kinetic coefficient (K)

From (13) we have:

$$lnK = -\frac{Q_{create\ phase}}{R}.\frac{1}{T} + const \quad (14)$$

do đó

$$\frac{Q_{create\ phase}}{R} = -\frac{dlnK}{d(1/T)} \approx tg\alpha \quad (15)$$

$Q_{create\ phase}$ from (15) is easily determined from the graph. Note that in this method it is necessary to determine K at different temperatures, but this temperature still has the same characteristics of n (same nucleation and nuclears development conditions). It can be determined precisely by equations with K at different temperatures
Determination of phase precipitation activity from phase transformation fraction (X)
From the empirical expression (2):

$$\ln\ln\frac{1}{1-X} = n\ln K + n\ln t \quad (16)$$

If X= const then:

*n*lnK +*n*lnt = const do đó

$$\frac{\partial lnK}{\partial(1/T)} = -\frac{Q_{create\ phase}}{R} + const \quad (17a)$$

$$\frac{\partial \ln K}{\partial(1/T)} = -\frac{\partial \ln t}{\partial(1/T)} + const \quad (17b)$$

Equilibrium (17a) & (17b) we get:

$$\frac{Q_{create\ phase}}{R} = \frac{\partial lnt}{\partial(1/T)} \quad (18)$$

In this method it is necessary to know t for some X at different temperatures and usually take the X where it is easiest to determine. Similar to the above, the phase transformation activity can be accurately determined by the equation from X = const at different temperatures.

RESEARCH RESULTS ON KINETICS OF PHASE PRECIPITATION DURING AGING

Determine the kinetic parameters of phase precipitation

Determination of phase transformation fraction (X) and phase transformation mechanism

To determine the phase transformation fraction (X), direct methods can be used: quantification of the phase fraction from the transmission electron microscopy image (if the precipitated phase size is less than 100 nm) and optical microscopy (if the emitted phase size larger than 10-5cm). In order to see the small-sized phases which increase mechanical properties (also the phases that need to be studied kinetics) in the aged aluminum alloy, it is not possible to use a small magnification optical microscope. The generally accepted direct method is transmission electron microscopy. The non-direct methods of determining the phase transformation ratio are: X-ray diffraction analysis, resistance measurement, hardness measurement, etc.

To determine the phase fraction by X-ray diffraction analysis, the more different the crystal structure and the crystal structure parameter from the matrix, the greater the symmetry of the precipitated phase, the greater the fraction , the easier it is to determine. However, for Al - Mg - Si alloys, the conditions for using X-rays are not favorable, especially the small fraction of phase precipitation. Thermal analysis is also a commonly used method to study phase transformation, but is often used to study in continuous heating and cooling processes [13], [14], [47], resistance measurement method in principle give the same results as hardness measurements. Therefore, in this study, the method of determining the phase transformation fraction (X) was selected from the hardness measurement.

Basis (1): from the relationship of the behaviour depending on the composition and the alloy microstructure of the phase diagram, it shows that if the alloy consists of two phases α and β, the hardness can be calculated according to the following formula:

$$HV_{material} = \% \alpha . HV_{\alpha} + \% \beta . HV_{\beta} \quad (19)$$

Therefore, if the alloy is in a state consisting of only two phases, the product and the matrix, the product phase fraction is easily determined from the hardness measurement, because:

Basis (2): by differential thermal analysis, DSC also determined that in the temperature range of $100^0C \div 175^0C$, when aging the Al-Mg-Si alloy, there is endothermic effect, proving that there is a phase transformation from higher energy phase to lower energy phase (from less stable phase to more stable phase). And also according to [13], [14], [47], the temperature range of $150^0C \div 200^0C$ can study aging by the mechanism: $\alpha_{oversaturation} \rightarrow \beta' \rightarrow \beta (Mg_2Si)$.

The β' phase has HVmax and the β phase (Mg2Si) appears after the hardness maximum.

On the other hand, [11] analyzes the results of the time-dependent hardness measurement on the table 3 and the figures (Figures 5 to 10) are graphs representing the dependence of the hardness on the aging temperature at a certain aging temperature, through which we see:

- Analysis of hardness value of alloy aging samples at different temperatures during 01h; 02h and 03h show that (Figures 6; 7; 8): When the aging temperature is increased from 120 đến 200ºC, the hardness value of the alloy sample increases very quickly from 75.21 to 83.46HV. However, if we continue to increase the natural aging temperature from 200 to 250ºC, the hardness value almost increases very slowly from 83.46 to 85.09HV, so it can be seen that here has not occurred the phase transformation for the alloy when doing aging. For the phase transformation here can only happen from $\alpha \rightarrow \beta'$.

- Analysis of Figures 8 and 9 when aging time is 04h and 05h at different temperatures shows: Initially, the aging temperature is 120ºC to 150ºC (5h) and 175ºC (4h), the hardness value increases gradually with aging temperature and reaches the maximum at this temperature; with values of 93.21HV and 94.72HV respectively. Continuing to increase the aging temperature, the hardness value decreases gradually. This is explained by the phase transformation $\alpha \rightarrow \beta'$, and after the maximum, phase transformation occurs $\beta' \rightarrow \beta (Mg_2Si)$.

- Continuing to increase the aging time up to 6h, the hardness value gradually decreased from 120ºC to 240ºC. This is explained by the grain coarsening of the β phases

Thus, from the analysis of hardness values, it is found that: If the aging time is 4h and 5h, the maximum hardness is about 175^0C (4h) and 150^0C (5h). This shows that the maximum is a phase transformation $\alpha \rightarrow \beta'$,and after the maximum is a phase transformation $\beta' \rightarrow \beta$ (Mg_2Si).

Table 3. HV hardness measurement result [MPa] depends on temperature and aging time

t°C / τ (h)	120	150	175	200	225	250
0	**46.38**	**46.38**	**46.38**	**46.38**	**46.38**	**46.38**
0,5	**63.52**	**71.25**	**69.21**	**79.27**	**80.5**	**80.95**
1	**75.21**	**77.15**	**81.22**	**83.46**	**84.16**	**85.09**
1,5	**77.11**	**79.45**	**90.21**	**89.91**	**88.73**	**89.56**
2	**81.31**	**85.32**	**89.89**	**92.27**	**92.18**	**95.37**
2,5	**83.06**	**85.14**	**93.38**	**93.76**	**95.74**	**96.32**
3	**85.61**	**86.61**	**94.12**	**98.09**	**99.12**	**99.85**
4	**86.18**	**89.51**	**94.72**	**93.34**	**92.61**	**92.32**
5	**89.05**	**93.21**	**92.65**	**90.15**	**87.12**	**86.25**
6	**93.48**	**92.13**	**91.32**	**89.12**	**87.45**	**85.15**
7	**91.82**	**89.88**	**90.95**	**96.56**	**79.32**	**77.82**
8	**90.15**	**87.32**	**90.15**	**83.89**	**78.15**	**76.32**

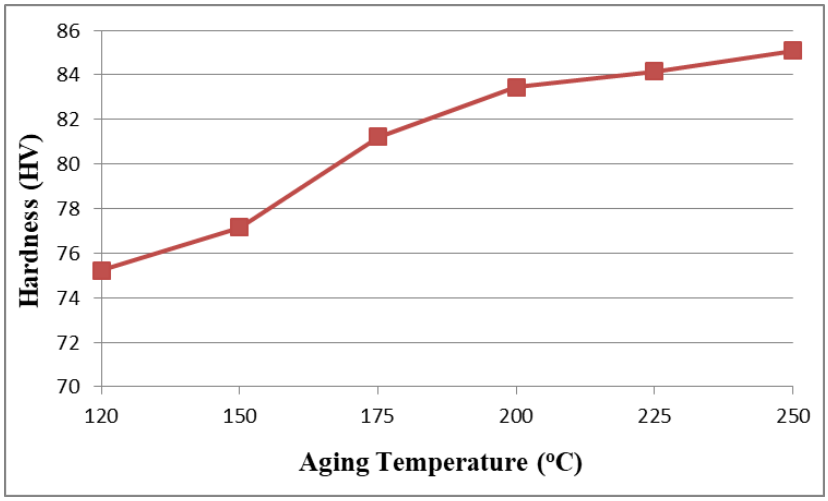

Figure 5. Hardness of the alloy at 1h aging, different temperatures *($\alpha_{qbh} \rightarrow \beta'$)*

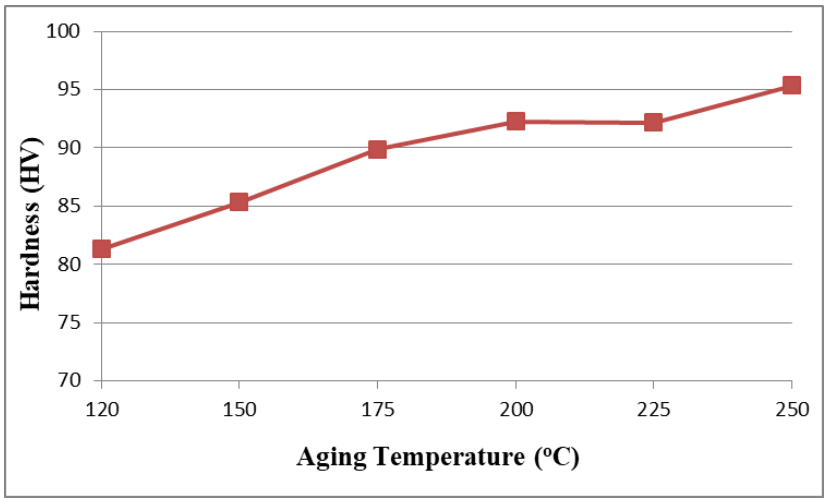

Figure 6. Hardness of 2h aged alloy at different temperatures *($\alpha_{qbh} \rightarrow \beta'$)*

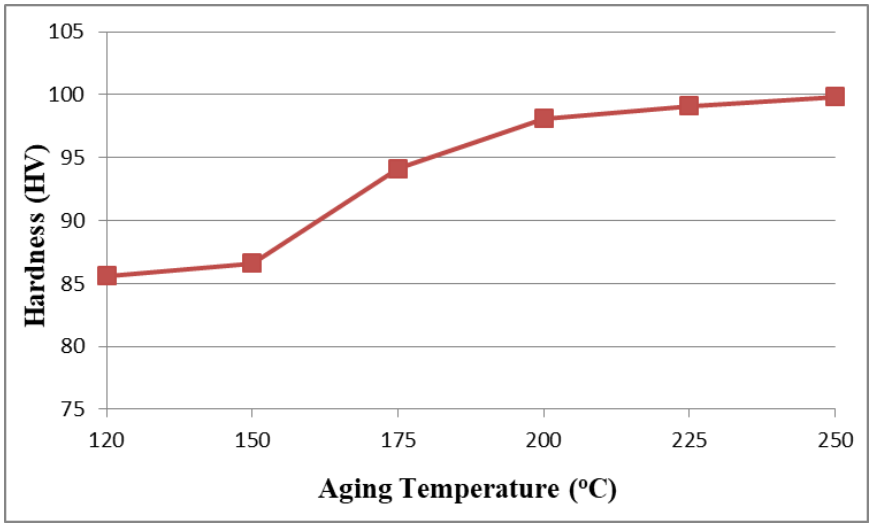

Figure 7. Hardness of 3h aged alloy at different temperatures ($\alpha_{qbh} \rightarrow \beta'$)

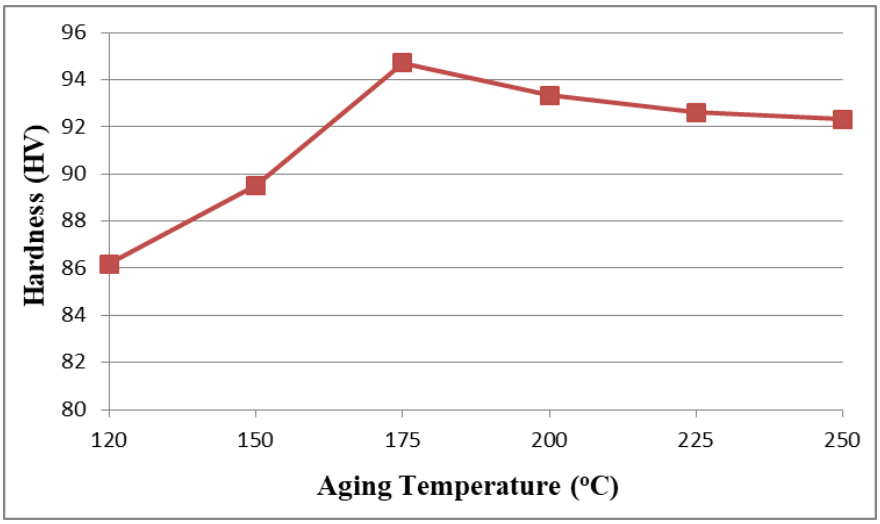

Figure 8. Hardness of 4h aged alloy at different temperatures at $t<175^0$ C ($\alpha_{qbh} \rightarrow \beta'$), ở $t > 175^0$C ($\beta' \rightarrow \beta$)

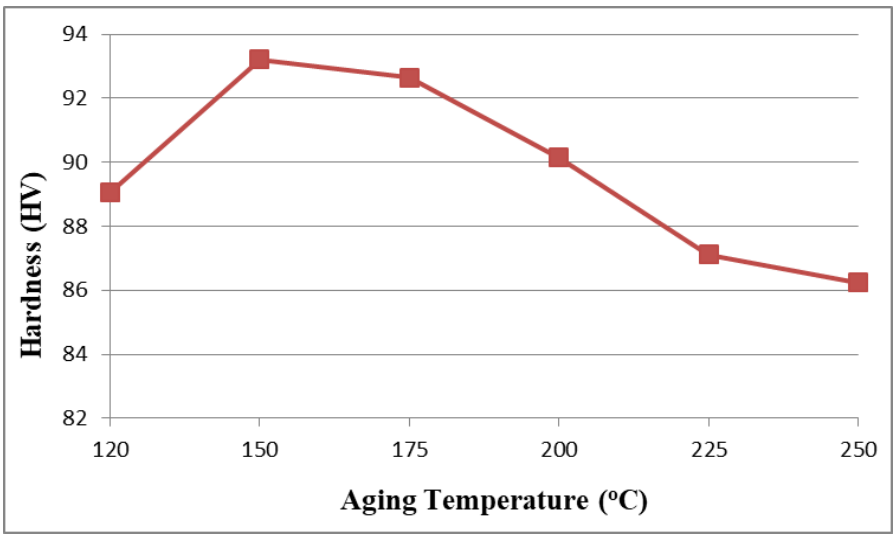

Figure 9. Hardness of 5h aged alloy at different temperatures at $t<150^0$ C ($\alpha_{qbh} \rightarrow \beta'$), ở $t > 150^0$C ($\beta' \rightarrow \beta$)

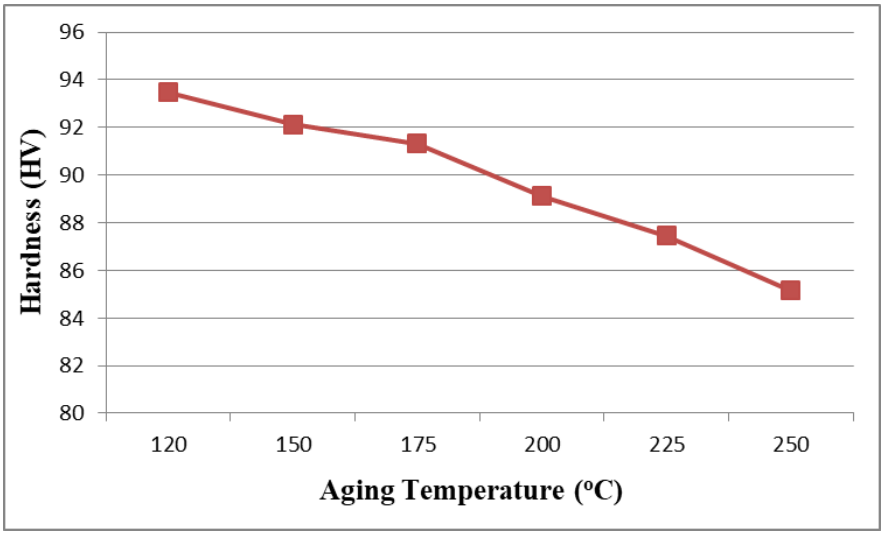

Figure 10. Hardness of 6h aged alloy at different temperatures $\beta \rightarrow \beta$ roughing)

Conclusion: The phase transformation mechanism in the studied temperature range is:

$\alpha_{oversaturation} \rightarrow \beta' \rightarrow \beta$ (Mg_2Si) and it is possible to determine the phase transformation fraction by the hardness method.

Determination of the dynamic coefficient (K and n)

K & n is determined from expression (3.17) as follows:

Convert the hardness measurement values (table 3) to the dimensionless code, if x = 1 corresponds to the maximum value (HVmax), and x = 0 corresponds to the minimum hardness (HVmin), the values of x_i (i = 1÷n, n is the number of samples) is determined as follows:

$$x_i = \frac{HV_i - HV_{\min}}{HV_{\max} - HV_{\min}} \tag{20}$$

Set y = lnln[1/(1-x)], x = lnt; b = n.lnK; a = n we have equation:

$$y = a.x + b \tag{21}$$

From the values of x_i calculated at the corresponding time t_i, we can determine the pair of values (x_i, y_i) according to (17). And from (21) determine the values of a and b from the experimental points (x_i, yi) by least squares method.

Let d_i be k=distance from the point (x_i, y_i) to the line (y =ax +b), we have:

$$d_i = \frac{|y_i - a.x_i - b|}{\sqrt{a^2 + 1}} \tag{22}$$

$$\sum_{i=1}^{n} d_i^2 = \frac{\sum_{i=1}^{n} \left(y_i - a.x_i - b\right)^2}{a^2 + 1} = F(a,b) \tag{23}$$

For $\sum_{i=1}^{n} d_i^2$ to be minimal, the partial derivative of F with respect to a and b must both be zero:

$$\frac{\partial F}{\partial a} = \frac{\partial F}{\partial b} = 0 \tag{24}$$

$$\frac{\partial F}{\partial a} = \sum_{i=1}^{n} \frac{2(a.x_i - y_i + b).(x_i + ay_i - ab)}{(a^2+1)^2} \tag{25}$$

$$\frac{\partial F}{\partial b} = \sum_{i=1}^{n} \frac{2(a.x_i - y_i + b)}{(a^2+1)} \tag{26}$$

Solving the system of equations (25) and (26), we have:

$$a.\sum_{i=1}^{n} x_i^2 - \sum_{i=1}^{n} x_i.y_i + b.\sum_{i=1}^{n} x_i + a^2.\sum_{i=1}^{n} x_i.y_i - a.\sum_{i=1}^{n} y_i^2 + 2.ab.\sum_{i=1}^{n} y_i - a^2 b\sum_{i=1}^{n} x_i - n.a.b^2 = 0 \tag{27}$$

$$n.b = \sum_{i=1}^{n} y_i - a.\sum_{i=1}^{n} x_i \tag{28}$$

Transforming (27) we have:

$$a.n.\sum_{i=1}^{n} x_i^2 - n.\sum_{i=1}^{n} x_i.y_i + b.n.\sum_{i=1}^{n} x_i + a^2.n.\sum_{i=1}^{n} x_i.y_i - a.n.\sum_{i=1}^{n} y_i^2 + + 2ab.n.\sum_{i=1}^{n} y_i - a^2.b.n.\sum_{i=1}^{n} x_i - n^2.a.b^2 = 0 \tag{29}$$

Substituting (28) into (29) we get:

$$a.n.\sum_{i=1}^{n} x_i^2 - n\sum_{i=1}^{n} x_i.y_i + \left[\sum_{i=1}^{n} y_i - a\sum_{i=1}^{n} x_i\right].\sum_{i=1}^{n} x_i + a^2.n.\sum_{i=1}^{n} x_i.y_i - a.n.\sum_{i=1}^{n} y_i^2 + + 2a.\left[\sum_{i=1}^{n} y_i - a\sum_{i=1}^{n} x_i\right].\sum_{i=1}^{n} y_i - a^2\left[\sum_{i=1}^{n} y_i - a\sum_{i=1}^{n} x_i\right].\sum_{i=1}^{n} x_i - a.\left[\sum_{i=1}^{n} y_i - a\sum_{i=1}^{n} x_1\right]^2 = 0 \tag{30}$$

Transforming (30) we get:

$$\left[n.\sum_{i=1}^{n} x_i.y_i - (\sum_{i=1}^{n} x_i).(\sum_{i=1}^{n} y_i)\right].a^2 + \left[(\sum_{i=1}^{n} y_i)^2 + n.\sum_{i=1}^{n} x_i^2 - (\sum_{i=1}^{n} x_i)^2 - n.\sum_{i=1}^{n} y_i^2\right].a + + (\sum_{i=1}^{n} x_i).(\sum_{i=1}^{n} y_i) - n.\sum_{i=1}^{n} x_i.y_i = 0 \tag{31}$$

Set:

$$A = \left[n.\sum_{i=1}^{n} x_i.y_i - (\sum_{i=1}^{n} x_i).(\sum_{i=1}^{n} y_i)\right] \tag{32}$$

$$B = \left[(\sum_{i=1}^{n} y_i)^2 + n.\sum_{i=1}^{n} x_i^2 - (\sum_{i=1}^{n} x_i)^2 - n.\sum_{i=1}^{n} y_i^2\right] \tag{33}$$

$$C = (\sum_{i=1}^{n} x_i).(\sum_{i=1}^{n} y_i) - n.\sum_{i=1}^{n} x_i.y_i \tag{34}$$

From (31) know A, B and C according to the values (x_i, y_i), calculation on excel we find a and b from the experimental values. That is to find the coefficients n, K in the kinetic equation of phase precipitation, the results in table 4.

Table 4: K phase precipitation rate constant, coefficient n

K,n \ t°C	120	150	175	200	225	250
K	**0.2682**	**0.2868**	**0.3127**	**0.3985**	**0.4431**	**0.5724**
N	**3.313**	**2.485**	**2.208**	**1.976**	**1.7019**	**1.204**

From Table 4 it can be commented:

Aging at the temperature of 175 ÷ 200^{0}C has n ≈ 2 and then according to [18], [23], [48] the geometry of β' is cylindrical, and all the nuclears are generated from the beginning, this result is also consistent with the published (e.g. [18], [23], [48]]) and is also consistent with the results of differential thermal analysis of the alloy studied.

• From the value of K at different temperatures, the phase transformation activity Q-phase can be determined from the expression:

$$k = const.exp(-\frac{Q_{create\ phase}}{RT} \quad (35a)$$

Thus: $$lnK = const(-\frac{Q_{create\ phase}}{R}.\frac{1}{T}) \quad (35b)$$

Then:

$$Q = \frac{d(\ln K)}{d(\frac{1}{T})}R \quad (36)$$

Or: $Q_{create\ phase}$ = - RT.lnK (37)

With R = 1,98 Cal/mol ≈ 0,9163 eV

Substituting the K values from table 4 received into (3.37) we can determine:

$Q_{create\ phase}$ = 4 kCal/mol = 17kJ/mol = 0.3 eV/atom.

This value is very small compared to the Q diffusivity of Mg, Si and Al in Al (in the condition of the vacancy in equilibrium), this comment is also found in publications [18], [23], [48]. It is explained that after quenching the vacancy concentration is large enough to increase the diffusion of the atoms, and there are soluble atom–empty pairs.

Determine K and n of strain sample ε = 5%, HGTN 0 h, HGNT at *175^{0}C*

From the results of measuring the hardness of 5% strain samples, direct normal aging then at 175^{0}C combined with using formulas 3.20 and 3.21 we have the results in Table 5:

Table 5 : Result of hardness measurement of 5% HGTN strain at 0 hours, HGNT at 175^{0}C

τ_{HGNT}(h)	HV_i	x_i	y_i	$x_i.y_i$	x_i^2	y_i^2
0,5	81,67	-	-	-	-	-
1	88,83	0,47	-0,45	-0,22	0,22	0,20
1,5	90,25	0,565	- 0,18	-0,1	0,32	0,033
2	93,19	0,759	0,35	0,267	0,576	0,124
2,5	94,86	0,87	0,71	0,616	0,755	0,50
3	96,85	1	3,57	3,656	1	12,71
4	96,07	0,95	1,089	1,032	0,9	1,18
5	95,54	0,913	0,9	0,82	0,84	0,80
6	93,62	0,787	0,44	0,35	0,62	0,19
7	93,0	0,746	0,32	0,24	0,56	0,199
8	90,47	0,58	- 0,14	- 0,08	0,336	0,020

Calculation based on the method of least squares presented in section 3, we find the values of a, b of equation That is to find K = 0.4813 and n = 1.932.

Comment :

With K determined, using formula (37) we can determine the phase transformation activity:

$Q_{create\ phase} = - RT.lnK$ (37)

= 2,53 kCal/mol = 0,2 eV/atom.

With R = 1,98 Cal/mol ≈ 0,9163 eV

Compared with the sample after quenching which do not deform, the phase precipitation energy in the sample after quenching with 5% strain is smaller. This can be explained by the dislocation (formed when deformed) has the effect of supporting the nucleation process and reducing the nucleation energy. When performing alloy deformation; the phases in the alloy have deformation; dislocation displacement and dislocation concentration in the grain boundary region. Therefore, the energy required to form the phase will decrease. Part of the energy of the phase generation was formed due to the formation of dislocation and dislocation concentration focus when straining. This pattern is explained by the formation of dislocation and displacement as follows:

Several studies on this model have been shown. As the study of Spingarn and Nix suggested that the grains rearrangement proposed by Ashby and Verral could not occur completely by diffusion. The work of Mishra et al. has shown that a small number of grains with small size of diffusion reduce stress in grains by grain boundary slip[49]–[51] (Figure 11).

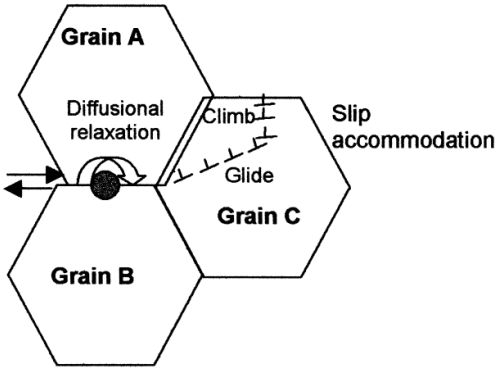

Figure 11. Grain boundary slip by grain boundary diffusion

A number of studies have shown that the displacement of the dislocations along the grain boundaries and the stress concentration at the grain boundary position is reduced due to the generation and displacement of the dislocations within the grain (figure 18). Figure 19 describes the model developed by Gifkins in the displacement of dislocations that take place in the residence region of the grain near the grain boundary [49]–[51].

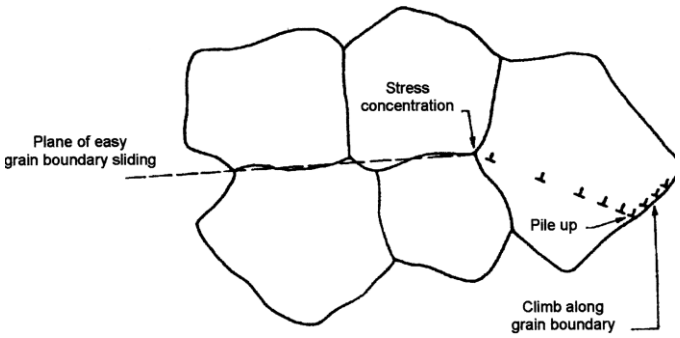

Figure 12. Ball-Hutchinson model of displacement of dislocations

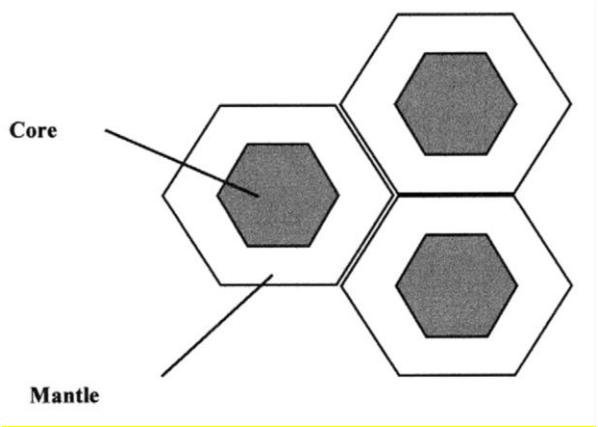

Figure 13. *Gifkins*' Core and residence region model

According to Fukuyo et al. [52], the mechanism of grain boundary slippage is the climb and displacement of the dislocation sequentially. At the recrystallization temperature, dislocation climbing at the grain boundary is due to a mechanism that adjusting the strain rate due to stress concentration. When the aging process is carried out, thanks to the appearance of dislocations when the grain is deformed, it will be formed by the following mechanism:

Al-Mg-Si alloy after cold plastic deformation combined with aging, when rolled, the grain will have the form of flakes or plates; when stretching, the grain is fibrous; when punching, the grain has a complex shape... As the degree of deformation increases, the free energy of the system increases and the strengthening effect of metal by causing lattice dislocation, reducing the stability of the oversaturated solid solution, increase in dislocation density (the dislocation density of aluminum alloy after annealing is about $10^7 \div 10^8$ cm^{-2}, when cold deformation of aluminum alloy is about $10^{10} \div 10^{11} cm^{-2}$), increase lattice defects... , that means accelerate the aging process. Combined with the change in the aging temperature, it will lead to a change in the microstructure and properties of the alloy when treated at different temperatures [53]–[62].

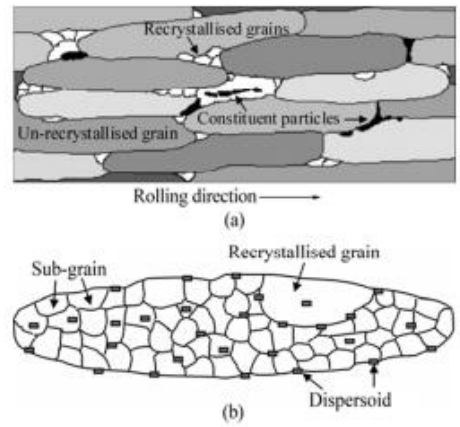

Figure 14. Model of alloy after deformation (a) and heat treatment (b)

CONCLUSION

1) In the aging temperature range of 120^0C, 150^0C, 175^0C 200^0C, Al - Mg - Si alloys precipitates phases according to the following mechanism:

$\alpha_{qbh} \rightarrow \beta' \rightarrow \beta$ (Mg_2Si) and grain coarsening.

2) K,n and Q of Al - Mg - Si alloy have been determined from hardness measurements at different aging temperatures and times.

- The results of determination of n ≈ 2 in the aging zone 175^0C ÷ 200^0C, combined with the method of differential thermal analysis, optical microscopy, show that the β' phase has a cylindrical shape and all the nuclears are generated immediately from the beginning.

- The K value increases with aging temperature, indicating that the higher the aging temperature, the more diffusion process increases.

- The value Q ≈ 4 Kcal/mol is small compared to the displacement energy of the vacancy in Al (~ 0,7 eV/atom) and very small compared to the diffusion activity of Al (~1,4 eV/ atom), this may be due to the oversaturated vacancy creating with impurities empty–impurity pairs.

3) When the sample is strained by 5%, the dislocation density is increased, the presence of dislocation supports the nucleation process when precipitating the phase, so the phase precipitation energy Q decreases.

4) The results of kinetic studies of aging process confirmed that the β' phase is cylindrical in shape and formed by nucleation from the beginning. This confirms that it is possible to improve the efficiency of strengthening by β' phase precipitation in alloys by techniques that allow to increase the density of nucleation centers (low-energy regions) such as dislocations, grain boundaries, super grain boundaries, defects, vacancies combinations, etc. Strain in thermomechanical technology is one of the most potential techniques.

REFERENCES

[1] A.S.M. Handbook, Alloy Phase Diagram, vol. 3. 1992.

[2] E.E. Moore et al., "Thermodynamic Modeling of the Al-Ce-Cu-Mg-Si System and Its Application to Aluminum-Cerium Alloy Design," J. Phase Equilibria Diffus., vol. 41, No. 6, 2020.

[3] L. Ding et al., "The structural and compositional evolution of precipitates in Al-Mg-Si-Cu alloy," Acta Mater., vol. 145, 2018.

[4] X. Yang et al., "Microstructural Evolution and Phase Transformation of Al–Mg–Si Alloy Containing 3% Li During Homogenization," in Springer Proceedings in Physics, vol. 217, 2019.

[5] O. Trudonoshyn, O. Prach, P. Randelzhofer, K. Durst, and Körner, "Heat treatment of the new high-strength high-ductility Al–Mg–Si–Mn alloys with Sc, Zr and Cr additions," Materialia, vol. 15, 2021.

[6] L. Hitzler et al., "Heat treatments and critical quenching rates in additively manufactured Al-Si-Mg alloys," Materials (Basel)., Vol. 13, No. 3, 2020.

[7] S. Toschi, "Optimization of a354 al-si-cu-mg alloy heat treatment: Effect on microstructure, hardness, and tensile properties of peak aged and overaged alloy," Metals (Basel)., Vol. 8, No. 11, 2018.

[8] E. Sjölander and S. Seifeddine, "The heat treatment of Al-Si-Cu-Mg casting alloys," Journal of Materials Processing Technology, Vol. 210, No. 10. 2010.

[9] R.V. Kumar, R. Keshavamurthy, C.S. Perugu, and C. Siddaraju, "Influence of heat treatment on microstructure and mechanical behaviour of hot-rolled Al-Mg-Si alloy," Adv. Mater. Process. Technol., 2020.

[10] D.N.N.X.D. Pham, A.T. Hoang, "A Study on the Effect of the Change of Tempering Temperature on the Microstructure Transformation of Cu-Ni-Sn Alloy," Int. J. Mech. Mechatronics Eng., Vol. 18, No. 04, Pp. 01–08, 2018.

[11] A.T. Hoang, L.H. Nguyen, and D.N. Nguyen, "A Study of Mechanical Properties and Conductivity Capability of CU-9NI-3SN ALLOY," 2018.

[12] X. Fan, Z. He, X. Kang, and S. Yuan, "Deformation and strengthening analysis of Al-Mg-Si alloy sheet during hot gas forming with synchronous die quenching," J. Manuf. Process., vol. 57, 2020.

[13] Y.B. Dong, W.Z. Shao, J.T. Jiang, D.Y. Chao, and L. Zhen, "Influence of quenching rate on microstructure and dimensional stability of Al–Cu–Mg–Si alloy," Mater. Sci. Technol. (United Kingdom), vol. 32, no. 18, 2016.

[14] M. Liu, Q. Guo, X. Zhang, M. Wüstenhagen, J. Čížek, and J. Banhart, “Clustering phenomena in quenched Al, Al–Mg, Al–Si and Al–Mg–Si alloys,” Scr. Mater., vol. 177, 2020.

[15] S. Pogatscher, H. Antrekowitsch, H. Leitner, D. Pöschmann, Z. L. Zhang, and P. J. Uggowitzer, “Influence of interrupted quenching on artificial aging of Al-Mg-Si alloys,” Acta Mater., vol. 60, no. 11, 2012.

[16] G. Gao, Y. Li, Z. Wang, H. Di, J. Li, and G. Xu, “Effects of the quenching rate on the microstructure, mechanical properties and paint bake-hardening response of Al-Mg-Si automotive sheets,” Materials (Basel)., vol. 12, no. 21, 2019.

[17] R.E. Smallman and R.J. Bishop, Modern Physical Metallurgy and Materials Engineering. 1999.

[18] C. Flament et al., “Stability of β″ nano-phases in Al-Mg-Si(-Cu) alloy under high dose ion irradiation,” Acta Mater., vol. 128, 2017.

[19] J. Du, A. Zhang, Y. Zhang, T. Wang, S. Xiong, and F. Liu, “Atomistic determination on stability, cluster and microstructures in terms of crystallographic and thermo-kinetic integration of Al−Mg−Si alloys,” Mater. Today Commun., vol. 24, 2020.

[20] F. García-Moreno et al., “The influence of alloy composition and liquid phase on foaming of Al–Si–Mg alloys,” Metals (Basel)., vol. 10, no. 2, 2020.

[21] L. Ding et al., “Study of the Q′ (Q)-phase precipitation in Al–Mg–Si–Cu alloys by quantification of atomic-resolution transmission electron microscopy images and atom probe tomography,” J. Mater. Sci., vol. 54, no. 10, 2019.

[22] L. Ding, H. Hu, Z. Jia, Y. Weng, X. Wu, and Q. Liu, “The disordered structure of Q′ and C phases in Al-Mg-Si-Cu alloy,” Scr. Mater., vol. 118, 2016.

[23] K. Inoue, K. Takata, K. Kazumi, and Y. Shirai, “High concentration of vacancies induced by β″ phase formation in Al–Mg–Si alloys,” Philos. Mag. Lett., vol. 100, no. 6, 2020.

[24] P. H. Ninive et al., “Detailed atomistic insight into the β″ phase in Al-Mg-Si alloys,” Acta Mater., vol. 69, 2014.

[25] S. J. Andersen, H. W. Zandbergen, J. Jansen, C. Træholt, U. Tundal, and O. Reiso, “The crystal structure of the β″ phase in Al-Mg-Si Alloys,” Acta Mater., vol. 46, no. 9, 1998.

[26] A. Afseth, J. H. Nordlien, G. M. Scamans, and K. Nisancioglu, “Effect of heat treatment on filiform corrosion of aluminium alloy AA3005,” Corros. Sci., vol. 43, no. 11, 2001.

[27] S. J. Andersen, C. D. Marioara, J. Friis, S. Wenner, and R. Holmestad, “Precipitates in aluminium alloys,” Adv. Phys. X, vol. 3, no. 1, pp. 790–814, 2018.

[28] D. Pottmaier et al., “The Brazilian energy matrix: From a materials science and engineering perspective,” Renewable and Sustainable Energy Reviews, vol. 19. 2013.

[29] E. P. Heikkinen, M. Iljana, And T. Fabritius, “Review on the phase equilibria in iron ore sinters,” ISIJ International, vol. 60, no. 12. 2020.

[30] I. L. Ferreira and A. Garcia, “The application of numerical and analytical approaches for the determination of thermophysical properties of Al–Si–Cu–Mg alloys,” Contin. Mech. Thermodyn., vol. 32, no. 4, 2020.

[31] M. J. Starink, L. F. Cao, and P. A. Rometsch, “A model for the thermodynamics of and strengthening due to co-clusters in Al-Mg-Si-based alloys,” Acta Mater., vol. 60, no. 10, 2012.

[32] Y. Weng, Z. Jia, L. Ding, S. Muraishi, X. Wu, and Q. Liu, “The multiple orientation relationships and morphology of β’ phase in Al-Mg-Si-Cu alloy,” J. Alloys Compd., vol. 767, 2018.

[33] A. Charlesby, “CRC materials science and engineering handbook,” Radiat. Phys. Chem., vol. 49, no. 2, 1997.

[34] W. D. Callister, Materials Science and Engineering, vol. 7. 2007.

[35] N. A. Belov, E. A. Naumova, T. K. Akopyan, and V. V. Doroshenko, “Phase diagram of Al-Ca-Mg-Si system and its application for the design of aluminum alloys with high magnesium content,” Metals (Basel)., vol. 7, no. 10, 2017.

[36] K. Chen et al., “Stabilizing Al–Mg–Si–Cu alloy by precipitation nano-phase control,” Mater. Sci. Eng. A, vol. 769, 2020.

[37] A. Zhu, B. M. Gable, G. J. Shiflet, and E. A. Starke, “Trace element effects on precipitation in Al-Cu-Mg-(Ag, Si) alloys: A computational analysis,” Acta Mater., vol. 52, no. 12, 2004.

[38] K. Kim et al., “Energetics of native defects, solute partitioning, and interfacial energy of Q precipitate in Al-Cu-Mg-Si alloys,” Acta Mater., vol. 154, 2018.

[39] H. Wang, H. J. Lin, W. T. Cai, L. Z. Ouyang, and M. Zhu, “Tuning kinetics and thermodynamics of hydrogen storage in light metal element based systems - A review of recent progress,” Journal of Alloys and Compounds, vol. 658. 2016.

[40] M. Zhang et al., “Optimization of heat treatment process of Al–Mg–Si cast alloys with Zn additions by simulation and experimental investigations,” Calphad Comput. Coupling Phase Diagrams Thermochem., vol. 67, 2019.

[41] F. Xu, X. Guo, P. Wu, J. Zhang, and Y. Deng, “Morphology Development and Kinetics of Plate or Rod Shaped Precipitates in Aluminum Alloys,” Xiyou Jinshu Cailiao Yu Gongcheng/Rare Met. Mater. Eng., vol. 46, no. 4, 2017.

[42] B. Zhang, L. Zhang, Z. Wang, and A. Gao, “Achievement of high strength and ductility in al-si-cu-mg alloys by intermediate phase optimization in as-cast and heat treatment conditions,” Materials (Basel)., vol. 13, no. 3, 2020.

[43] P. P. Seth, O. Parkash, and D. Kumar, “Structure and mechanical behavior ofin situdeveloped Mg2Si phase in magnesium and aluminum alloys - a review,” RSC Advances, vol. 10, no. 61. 2020.

[44] B. Lu, Y. Li, Y. Wang, X. Qian, G. Xu, and Z. Wang, “Effect of second-phase particle evolution in a twin-roll-casted Al-Mg-Si alloy on recrystallization texture and mechanical anisotropy,” Mater. Charact., vol. 176, 2021.

[45] E. Cerri, M. T. Di Giovanni, and E. Ghio, “A study of intermetallic phase stability in Al-Si-Mg casting alloy: The role of Cu additions,” Metall. Ital., vol. 112, no. 7–8, 2020.

[46] Z. Yang et al., “Natural ageing clustering under different quenching conditions in an Al-Mg-Si alloy,” Scr. Mater., vol. 190, 2021.

[47] I. Benariev, Y. A. Puchkov, G. G. Klochkov, Y. V. Loshchinin, and S. V. Sbitneva, “Effect of Cooling Rate under Quenching on the Structure and Properties of Sheets Made of High-Tech Alloy V-1341 of the Al–Mg–Si System,” Inorg. Mater. Appl. Res., vol. 11, no. 1, 2020.

[48] H. Mao et al., “β’’ needle-shape precipitate formation in Al-Mg-Si alloy: Phase field simulation and experimental verification,” Comput. Mater. Sci., vol. 184, 2020.

[49] R. S. Mishra, R. S. Haridas, and P. Agrawal, “High entropy alloys – Tunability of deformation mechanisms through integration of compositional and microstructural domains,” Materials Science and Engineering A, vol. 812. 2021.

[50] R. S. Mishra and A. K. Mukherjee, “Analysis of the role of grain size on superplasticity of γ titanium aluminides,” J. Mater. Sci., vol. 35, no. 1, 2000.

[51] R. K. Mishra, “Microstructure of hot-pressed and die-upset NdFeB magnets,” J. Appl. Phys., vol. 62, no. 3, 1987.

[52] H. Fukuyo, H. C. Tsai, T. Oyama, and O. D. Sherby, “Superplasticity and Newtonian-viscous Flow in Fine-grained Class I Solid Solution Alloys,” ISIJ Int., vol. 31, no. 1, 1991.

[53] N. R. Bochvar et al., “The effect of transition metals on the structure and hardening of Al-Mg-Si alloys after cold plastic deformation,” in Journal of Physics: Conference Series, 2020, vol. 1431, no. 1.

[54] B. Gruber et al., “Room temperature recovery of cryogenically deformed aluminium alloys,” Mater. Des., vol. 193, 2020.

[55] J. A. Omotoyinbo, I. O. Oladele, and W. Shokoya, “Effect of the degree of plastic deformation on the electrical resistance and thermal conductivity of Al-Mg-Si alloy,” Leonardo Electron. J. Pract. Technol., vol. 13, no. 24, 2014.

[56] J. Hu, W. Zhang, D. Fu, J. Teng, and H. Zhang, “Improvement of the mechanical properties of Al-Mg-Si alloys with nano-scale precipitates after repetitive continuous extrusion forming and T8 tempering,” J. Mater. Res. Technol., vol. 8, no. 6, 2019.

[57] M. S. Tsai, P. L. Sun, P. W. Kao, and C. P. Chang, “Influence of severe plastic deformation on precipitation hardening in an Al-Mg-Si Alloy: Microstructure and mechanical properties,” Mater. Trans., vol. 50, no. 4, 2009.

[58] J. M. Sanchez, I. Vicario, J. Albizuri, T. Guraya, and E. M. Acuña, “Design, Microstructure and Mechanical Properties of Cast Medium Entropy Aluminium Alloys,” Sci. Rep., vol. 9, no. 1, 2019.

[59] C. Gode, “Influence of a low-temperature Plastic-deformation process on the microstructure of an Al-Si-Mg aluminum alloy,” Mater. Tehnol., vol. 55, no. 2, 2021.

[60] X. Zhang, X. Zhou, J. O. Nilsson, Z. Dong, and C. Cai, “Corrosion behaviour of AA6082 Al-Mg-Si alloy extrusion: Recrystallized and non-recrystallized structures,” Corros. Sci., vol. 144, 2018.

[61] H. J. Roven, M. Liu, and J. C. Werenskiold, “Dynamic precipitation during severe plastic deformation of an Al-Mg-Si aluminium alloy,” Mater. Sci. Eng. A, vol. 483–484, no. 1-2 C, 2008.

[62] E. A. Mørtsell et al., “The effect of elastic strain and small plastic deformation on tensile strength of a lean Al-Mg-Si alloy,” Metals (Basel)., vol. 9, no. 12, 2019.